ADVANCED MATERIALS
www.advmat.de
Materials Views
www.MaterialsViews.com

COMMUNICATION

Generating Switchable and Reconfigurable Optical Vortices via Photopatterning of Liquid Crystals

Bing-yan Wei, Wei Hu, Yang Ming, Fei Xu, Sam Rubin, Jian-guo Wang, Vladimir Chigrinov, and Yan-qing Lu**

Optical vortices have attracted intensive attention and been extensively studied during the past two decades.[1–3] The optical vortex is a light beam characterized by a helical phase front.[4] This means that the wavefront is twisted like a corkscrew around its axis of propagation (**Figure 1**a). The number of phase windings in a single wavelength is called the topological charge m, which directly reveals the velocity of the phase rotation around the axis. To ensure the continuity of the field, m must be an integer for an optical vortex. That implies the quantization of the orbital angular momentum (OAM).[2] The phase singularity at the axis dictates zero intensity, which leads to a donut-like intensity distribution (Figure 1b). The topology of the ring's spatial shape is determined by the topological charge. The topological charge and corresponding OAM add a new degree of freedom to characterize the properties of a light beam, thus opening a door towards widespread applications even in some uncharted territories.[3,5] Theoretically, optical vortices have an infinite number of states due to the unlimited topological charge.[6] Thanks to the large number of vortical states, OAM multiplexing could be utilized in quantum computing,[3,7] which uses the multistate of light to encode and store information. Meanwhile, it supplies a higher bandwidth of information, which could increase the radio spectral efficiency and show great potential for the cryptography community as well.[8] When used as optical tweezers, optical vortices will induce torque on electric dipoles besides the trapping caused by the optical gradient force, making the rotation control of particles possible.[9] Based on this property, OAM driven micromachines such as micro-motors and micro-propellers have been created,[5] which facilitate the precisely multi-dimensional manipulation of fine objects, such as microspheres and DNA. In astronomy, optical vortex coronagraphs are used to block the strong background light to increase the contrast of astronomical observations, which are useful for the search of extrasolar planets.[10] In all, optical vortices have broad applications in the fields of informatics, micro-manipulation, and astronomy.[5,8,10]

So far, several techniques have been developed to generate optical vortices. In the initial research, a mode converting strategy was used.[2,11] However, its optical setup is bulky and complex, which is inconvenient in the generation of beam vortices with large m numbers. The most straightforward approach to generate an optical vortex is through direct rephasing of a plane wave using a spiral phase plate.[12] An extreme precision in the pitch of helical surface and optical thickness at different azimuthal position is required for this strategy.[13] Q-plate, an inhomogeneously birefringent wave plate with specified geometry of the local optical axis, has also been used for the vortex generation.[14–16] Apart from the above setups and elements, another alternative choice is "fork" grating, a diffraction grating with dislocations centered at the beam axis.[17] The fork grating can convert a Gaussian beam into a series of helically phased beams with opposite twist directions. This is a very convenient approach for generating beam vortices at present. To accomplish a tunable vortex generator, which is especially required in the fields of OAM based quantum computing, optical communicating and micromanipulating, liquid crystals (LCs), exhibiting excellent electro-optical (EO) properties and widely used in nondisplay fields,[18] have been introduced.[15,19] Typically, patterned electrodes[20] and polymer dispersed LCs[21] are used to produce the fork gratings, however, the geometry of such gratings are fixed thus their output topological charge could not be changed. For a commercially available spatial light modulator (SLM), usually a reflective liquid crystal display controlled by a computer, could generate arbitrary holograms including fork gratings.[22] Unfortunately, they are commonly designed for visible light and suffer from polarization sensitivity, low optical efficiency, and slow switching. Therefore, new alternative techniques for generating fast switchable, reconfigurable, wavelength and polarization insensitive optical vortices in high quality and efficiency are in urgent demand. In this paper, by means of Digital Micro-mirror Device (DMD) based microlithography, a transmissive beam vortex generator overcoming all the above drawbacks is demonstrated.

Specially designed computer-generated holograms can convert a Gaussian laser beam into a desired helical mode. The helical wavefront of an optical vortex can generally be described by the phase function $\Psi_1 = \exp(im\theta)$ (Figure 1a), where θ is the azimuthal angle of a cylindrical coordinate system (r, θ, z) around the z axis, which indicates the beam propagation direction, m is the topological charge and can be positive or negative, depending on the direction of the twist (positive for counterclockwise rotation and negative for clockwise rotation).

B.-y. Wei, Prof. W. Hu, Y. Ming, Prof. F. Xu, Prof. Y.-q. Lu
National Laboratory of Solid State Microstructures and College of Engineering and Applied Sciences
Nanjing University
Nanjing, 210093, China
E-mail: huwei@nju.edu.cn; yqlu@nju.edu.cn
S. Rubin, Dr. J.-g. Wang
Thorlabs China
Shanghai, 200331, China
Prof. V. Chigrinov
Center for Display Research
Department of Electronic and Computer Engineering
Hong Kong University of Science and Technology
Clear Water Bay, Kowloon, Hong Kong, China

DOI: 10.1002/adma.201305198

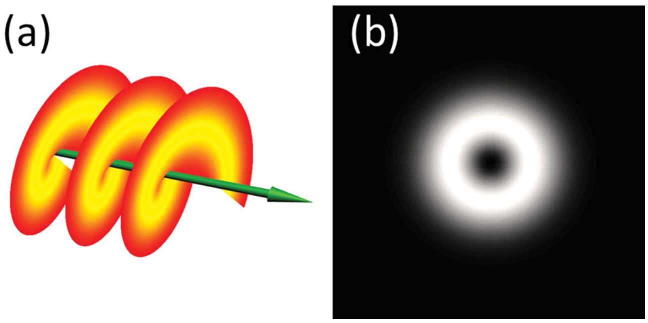

Figure 1. a) The helical wave fronts of a vortex beam with $m = 1$ calculated according to $\Psi_1 = \exp(im\theta)$. The arrow indicates the beam propagation direction. The color represents the light intensity, red means weak whereas yellow means strong. b) Normalized intensity distribution when the beam is viewed against the propagation axis.

To imprint a phase Ψ_1 in a Gaussian beam, the interference of a reference tilted plane wave $\Psi_2 = \exp(ikx)$ (where k is the spatial frequency indicating the tilting angle of the wave) and the object wave Ψ_1 is utilized to form the computer-generated holograms. The interference pattern could be described by the function,[16]

$$H = |\Psi_1 + \Psi_2|^2 = \left|\exp(im\theta) + \exp(ikx)\right|^2 = 2[1 + \cos(kx - m\theta)] \quad (1)$$

where $\theta = \tan^{-1}(y/x)$ is the polar coordinate. **Figure 2** shows the calculated computer-generated hologram plots of H for (a) $m = 1$ and (b) $m = 2$, respectively. The holograms look like forks, with branchings in the central fringe. The patterns carry information of the topological charge m and the reference wave. When one of them is illuminated by a Gaussian beam $\Psi_G = \exp(-r^2/w^2)$ of width w, the resulting far-field Fraunhofer diffraction pattern is proportional to the Fourier transform F of the product of the input function Ψ_G and the hologram transmission function H. As a consequence, the irradiance in a plane far from the fork grating is given by,[16]

$$I = F[\Psi_G H] = F[\exp(-r^2/w^2)\left|\exp(im\theta) + \exp(ikx)\right|^2] \quad (2)$$

where k_x is the x-component of the wave vector of the titled wave. The beam is thus reconstructed and the vortices are produced in the diffraction orders of the output beam. A contour plot of the function I can be calculated and one of them, for $m = 1$, is plotted in Figure 1b.

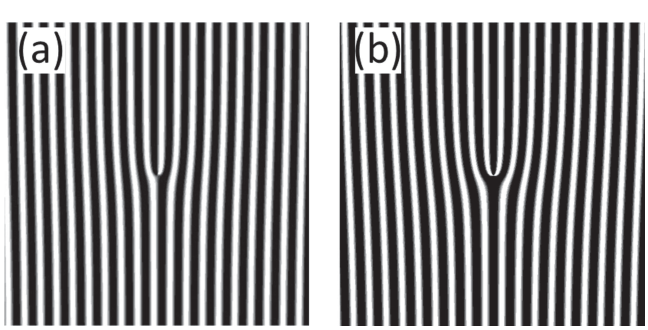

Figure 2. Computer-generated holograms calculated according to Equation (1) for a) $m = 1$ and b) $m = 2$.

A photoalignment technique and a DMD based micro-lithography system were employed to transfer the computer-generated holograms into LC cells to locally control the LC directors. Compared to traditional rubbing, photoalignment is much more suitable for high-resolution multi-domain alignments.[23] By means of this technique, high-quality LC alignment with a resolution of up to 1 μm has been shown.[24] Here we used sulphonic azo-dye SD1 (Chemical structure as shown in Figure S1) as the alignment material. Under UV exposure, the dye molecules tend to reorient their absorption oscillators perpendicular to the UV light polarization because of the isomerization of azo groups and dichroic absorption of the chromophores. The orientation of SD1 will spread to adjacent LC molecules thus guiding the LC directors. SD1 is rewritable and only the last photo-reorientation will be recorded, which drastically facilitates the patterning. As we know, optical approaches are broadly used in microfabrication. In our work, a DMD (1024 × 768, Discovery 3000, Texas Instruments) was utilized as a dynamic mask.[25] The DMD consisted of 786 432 pixelated micro-mirrors, and each mirror can be independently tilted by an electrostatic force thus redirecting the reflected wave propagation. Consequently, the desired light pattern can be generated through simple image input on a computer.

The setup is schematically illustrated in **Figure 3**. A uniform and collimated light beam from a mercury lamp (S1000, EXFO, Canada) illuminates onto the DMD and carries on the designed fork grating hologram. After being polarized, the beam is focused by a 10× objective and then the microimage is recorded on the substrate. Moreover, a CCD is utilized to monitor the focusing of the image.[25] This setup could output images with a resolution down to ca. 1 μm (10 times smaller than the size of a single micromirror), which is close to SD1's spatial resolution limit. Moreover, the image could be projected exactly at the SD1 layer even for very thick cell substrates, which avoids the pattern deformation of fixed masks due to the beam expanding. Very fine alignment microstructures could thus be obtained.

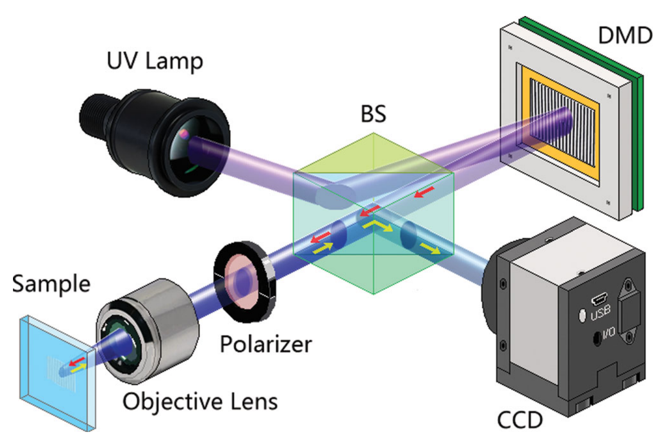

Figure 3. Schematic illustration of DMD based micro-lithography setup. It consists of a light emission part, a dynamic pattern generation part, an image focusing part and a monitor part, all of which work together to provide a faithful image transfer on the substrate. DMD: digital micromirror device, BS: beam splitter, CCD: charge coupled device. Red and yellow arrows indicate the propagations of the projecting and monitoring light beams, respectively.

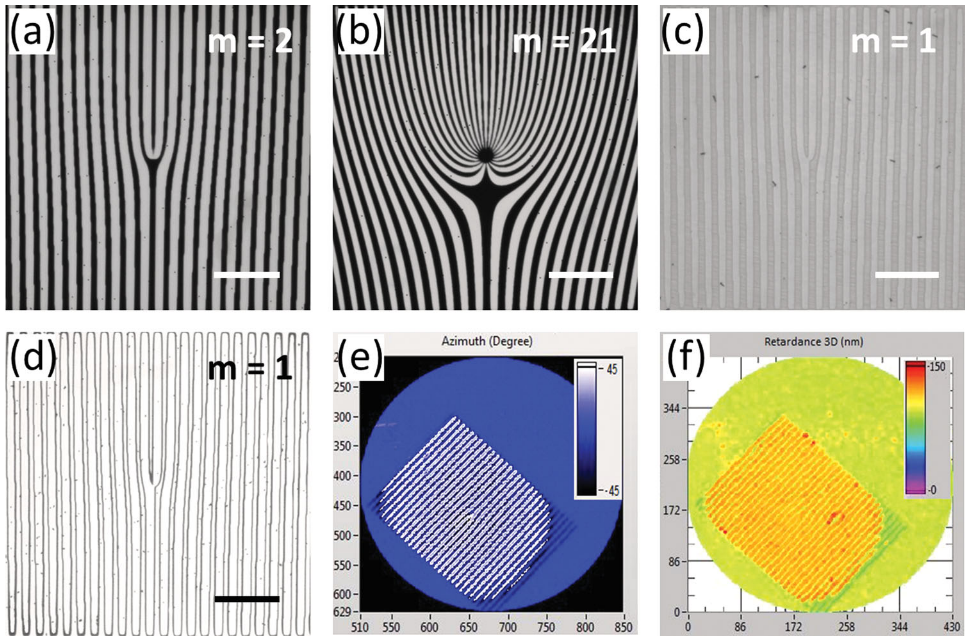

Figure 4. Micrographs of: TN/PA LC fork gratings with a) m = 2 and b) m = 21, c) an orthogonal HAN and d) PA fork grating respectively. e,f) The azimuth (e) and phase retardance (f) distributions of the sample shown in (d). The scale bar is 100 μm. All the cells are infiltrated with LC E7. All micrographs are taken under a cross-polarized microscope.

A two-step photo-exposure process was performed to construct the micro-pattern.[26] The cell was uniformly exposed with linearly polarized light firstly, and then the same cell was then rotated 90 degrees and exposed again to receive the hologram pattern generated by the DMD system. The exposed areas were realigned to be orthogonal to the orientation of the shadow areas. Fork gratings were thus fabricated after the LC was capillarily filled.

To facilitate the observation, fork gratings were demonstrated by deploying a nematic LC on alternative twisted nematic (TN) and planar aligned (PA) (i.e., homogeneously aligned) domains. Herein, the computer-generated hologram with designed topological charge was recorded on a homogeneously pre-aligned substrate, then the substrate was assembled with another homogeneously aligned one to form the cell. **Figure** 4a and b exhibit the micrographs of TN/PA bi-domain LC fork gratings with m = 2 and m = 21 respectively under a cross-polarized microscope. A polarizer is fixed parallel to the LC director at the input end. In this condition, the polarized light follows the twisted orientation of the LC and alters its polarization by 90° in the TN regions and totally passes through an analyzer. Therefore, these domains exhibit a bright state. However, in the PA regions, the light does not change its polarization and is blocked by the analyzer after passing through the regions, inducing a dark state. The micrograph in Figure 3a reveals a faithful replica of the computer-generated hologram as shown in Figure 2a.

Compared to the amplitude modulation of the above TN/PA fork gratings, phase modulation should supply a much higher efficiency. Figure 4c shows a fork grating consisting of two complementary hybrid aligned nematic (HAN) domains. For this cell, the orthogonal PA fork grating pattern was recorded on an SD1-coated substrate, whereas a polyimide layer was coated on the other substrate and uniformly rubbed at 45° with respect to both above PA orientations to perform a homeotropical alignment. LC fork gratings with an orthogonal PA hologram pattern recorded on both subtrates are also demonstrated. Figure 4d presents an orthogonal PA fork grating with m = 1. From Figure 4c and d, it can be seen that two adjacent regions are quite uniform in brightness except for some boundary lines. The uniformity proves the high quality and excellent orthogonality of the alignments. The occurrence of boundary lines is related to the desclination between the adjacent heterogeneous orientations.[27] Figure 4e and f present the azimuth and phase retardance distributions, respectively, of the LC fork grating shown in Figure 4d. The two pictures were calculated from a two-dimensional Stokes parameters measurement of the output optical image, which reveals that both the alignment and phase retardance have been presicely controlled. Some non-uniformity is observed on the edge of the fork gratings because of the comparably weak intensity of the collimated beam there. The SD1 is compatible to most liquid crystals and can be utilized in any LC alignment mode to take the place of the traditional planar alignment layers.

Several tests were carried out on an orthogonal HAN (or-HAN) fork grating with m = 1 to find out its performance. A laser beam with λ = 671 nm illuminated the sample and its diffraction patterns were captured by a CCD. The optical vortices were observed in the diffraction orders on both sides of order 0^{th}. The topological charges of these optical vortices are given by nm, where n represents the diffraction order and m is the charge of the LC fork grating. Here, only the $\pm1^{st}$ orders are considered because of their highest efficiency. **Figure** 5a and b reveal the top and front view of 0^{th} and $\pm1^{st}$ orders. The pictures were taken at an applied voltage of 1.7 V_{rms}, which is the "on" state of the optical vortex. Under this condition, the

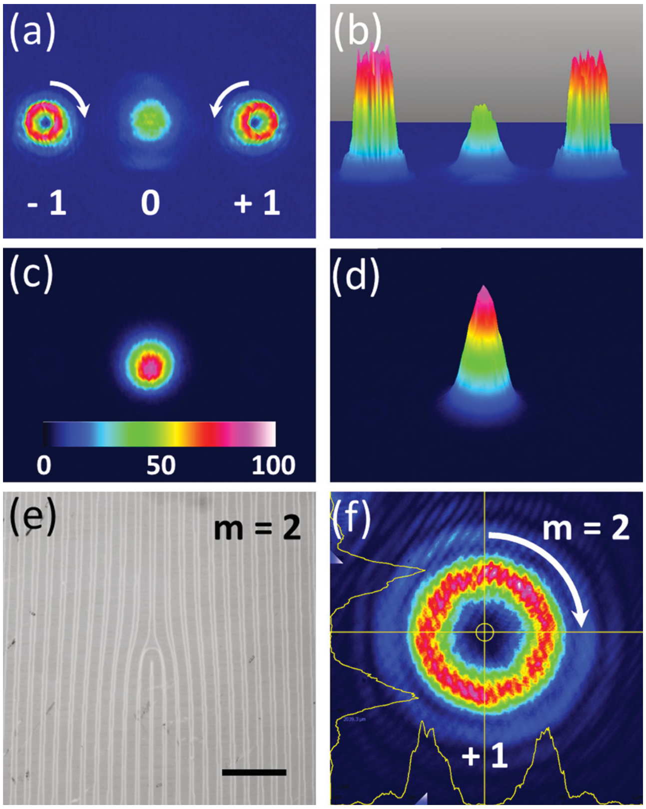

Figure 5. a–d) Diffraction patterns from the traversal of a laser through an or-HAN LC fork grating with m = 1. a) Top view and b) front view of the 0th and ±1st orders during the "on" state of the optical vortex; c) Top view and d) front view of the same orders in the "off" state. e) Micrograph of a fork grating with m = 2 reconfigured from one with m = 1. f) The optical vortex at 1st diffraction order from the sample given in (e). Arrows indicate the twist direction of the vortex. A color bar was inserted in (c), which indicates the relative optical intensity in all diffraction patterns.

phase retardation between the o-ray and e-ray is π, thus supplying the maximum diffraction efficiency. Clear optical vortices with designed topological charges were obtained and most of the energy was distributed to the diffraction orders. When the applied voltage was increased to 10 V_{rms}, the phase retardation was reduced to nearly zero, thereby the ±1st orders were highly suppressed, leaving only a standard Gaussian beam in the center as shown in Figure 5c and d. This is the "off" state of the optical vortex. The dielectrical and optical anisotropies of LCs make LC molecules respond to external stimulus. Thus, dynamic switching between Gaussian modes and vortex beams is achieved through changing the applied voltages.

Thanks to the excellent optical rewritability of SD1 caused by their reversible isomerization, the hologram pattern could be erased by a uniform linearly polarized light and then rewritten by the DMD system to form a new hologram with different m. In our experiments, we erased the above m = 1 fork grating and rewrote another one with m = 2 as given in Figure 5e. The spatial shape of the 1st order vortex is presented in Figure 5f. The horizontal and vertical section lines in Figure 5f depict the corresponding intensity profiles. Because of their different topological charge, the topology of the ring is different from the previous one, and the black hole became larger. Moreover, the twist direction was opposite to that of the previous grating because of the inversion of the fork pattern. Herein, both the topological charge and the twist direction of a given diffraction order was reconfigured by light. This is enormously significant as it means that we can manipulate the OAM arbitrarily and instantly, which will facilitate broad applications from particle trapping and secure communicating to quantum computing. By the way, because of the rewritability of SD1, direct exposure to any strong UV light should be avoided during storage. However, both the light and thermal stabilities of the cells were good at ambient conditions. Our earliest samples endured heating (over 100 °C), EO measurements, and microscope observations for several times during the past 8 months, and they still work well and no obvious decay has been observed.

Curves of voltage-dependent efficiency (V–η curves) of the 1st order optical vortex of an LC fork grating (orthogonal HAN, m = 1) are plotted in **Figure 6**a. Here, the efficiency is defined as the intensity ratio of the 1st diffraction order to the total incident light. As shown in Figure 6a, the V–η curves at three different wavelengths, 671 nm, 632.8 nm and 532 nm, are exhibited. All

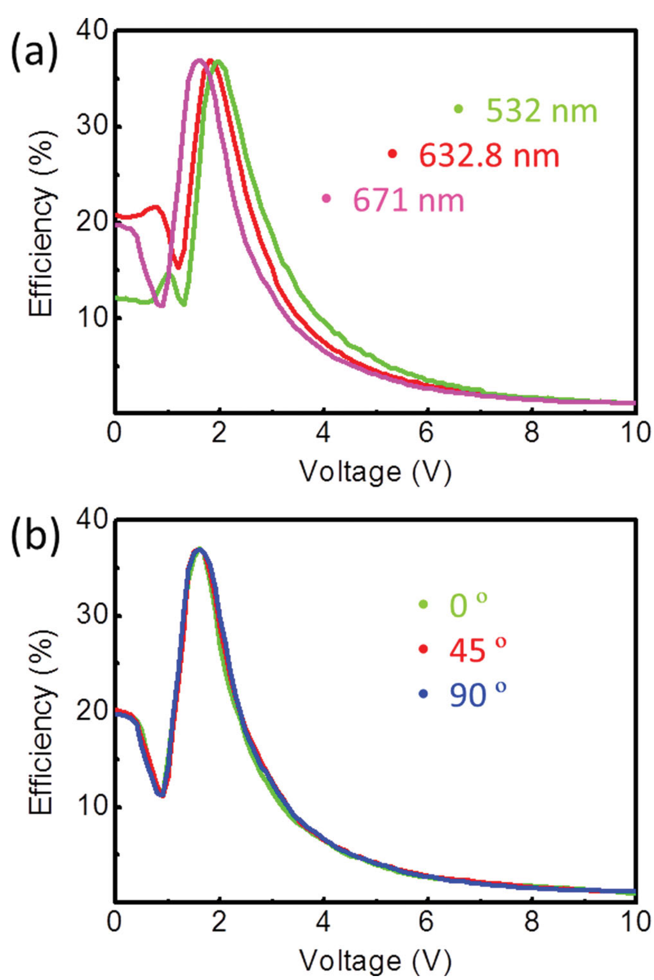

Figure 6. V–η curves of the 1st order optical vortex of an or-HAN LC fork grating with m = 1 at a) different incident wavelengths: 532 nm, 632.8 nm and 671 nm; and b) different incident polarization angles: 0°, 45°, and 90°.

η maxima reach around 37%, that is 74% of that of ±1st orders. In addition, some energy has been distributed to higher orders. That is consistent with the energy distribution given in Figure 5b. It suggests our samples exhibit good tolerance to incident light wavelength, and equivalent high efficiencies could be achieved using different wavelengths by slightly tuning the applied voltage. This effectively eliminates the cost of preparing different elements for different wavelengths. Because of the unique cell configuration (the VA alignment layer is rubbed at 45°), both the polar and azimuthal angles were changed by the applied voltage, therefore the V–η curves were anomalous before the "on"-state voltage. V–η curves of different incident polarization angles, 0°, 45° and 90°, are also shown in Figure 6b. Excellent polarization independency is exhibited from the complementary or-HAN cell as the two perpendicular components derived from all incident light experience a same refractive index change.[27] The V–η curves are quite similar when rotating the sample, indicating that the samples exhibit excellent polarization independency to normally incident light. This meets another key requirement for common optical devices. The EO response of this sample was also measured. We defined the ON/OFF time as the duration that the intensity of the 1st order optical vortex changes from 10% to 90% and reverse. The measured values are 21 ms and 1 ms separately at a voltage alternating between 1.7 V and 15 V. The response time could be further reduced through decreasing the cell gap. From our estimation, the smallest cell gap possible whilst still keeping a high diffraction efficiency is 3 μm (The relationship between cell gap and diffraction efficiency is given in Section 1 of the Supporting Information). In this case, the EO response could be much faster. A dual-frequency LC was infiltrated into or-HAN cells with fork grating patterns as well and their EO properties were measured (Figure S1, Supporting Information). At an optimized cell gap, switching between ON and OFF was accomplished through applying a 15 V signal with alternating frequency between 1 kHz and 80 kHz. These samples supplied a fast EO response down to the submillisecond scale for both switching on and off. (Details are given in Section 2 of the Supporting Information)

We have demonstrated LC fork gratings in various alignment modes with arbitrary topological charges through photopatterning utilizing a DMD-based microlithography system. These fork gratings exhibit high alignment quality, excellent phase retardance uniformity as well as other advantages such as easy fabrication, simple configuration, high resolution, light weight and low cost. Optical vortices generated from these fork gratings reveal high efficiency, wide operating spectrum range, and excellent polarization independency. The characteristics of electrical tunability and optical reconfigurability endow the LC fork gratings with great potential for a wide range of applications. As SD1 is suitable to the planar orientation of most kinds of liquid crystals, reducing the EO response down to the submillisecond or even microsecond level is accomplishable by introducing dual frequency,[27] polymer network,[28] or ferroelectric[29] liquid crystals.

Experimental Section

Chemicals and reagents: Indium-Tin-Oxide (ITO) coated glass substrates were first cleaned in an ultrasonic bath, then UV-ozone cleaned, and then spin-coated with 0.5% solution of sulphonic azo-dye SD1 (Dai-Nippon Ink and Chemicals, Japan) in dimethylformamide (DMF). A polyimide (PI-5661, Nissan, Japan) was spin-coated for homeotropical alignment. All cells were infiltrated with LC mixture E7.

Photoalignment and cell assembling: SD1-coated substrates were irradiated by linearly polarized blue light (405 ± 10 nm) to create a uniform planar alignment with a dose of ca. 5 J cm^{-2}. Two substrates were then chosen according to the desired alignment modes. 6 μm spacers were sputtered over one substrate after which the other substrate was put on top of the spacers. The cell was thus assembled and sealed with epoxy glue. Then the cell was placed at the image plane of the DMD-based microlithography system to record the designed computer-generated hologram pattern. It was exposed to the same dose of linearly polarized blue light as above. The incident polarization was kept perpendicular to that of the pre-exposure. After the capillary filling of the LC, the desired fork grating was achieved.

Characterizations: The setup for the measurement of the two-dimensional Stokes parameters consisted of a polarizer, $\lambda/4$ plate, holder for the samples, another $\lambda/4$ plate, and a polarizer in sequence. A CCD camera was used as a two-dimensional detector array for the simultaneous detection of all four Stokes parameters of the output optical image.

Supporting Information

Supporting Information is available from the Wiley Online Library or from the author.

Acknowledgments

This work is sponsored by 973 programs (Nos. 2011CBA00200 and 2012CB921803), the National Natural Science Foundation of China (No. 11304151), Ph.D. Programs Foundation of the Ministry of Education of China (No. 20120091120020), and the Program for Changjiang Scholars and Innovative Research Team in University. Yan-qing Lu appreciates the support from the National Science Fund for Distinguished Young Scholars (61225026). The authors thank Prof. Xiao-shun Jiang for his constructive advice during manuscript preparation, Hao Qian and Guang-hao Shao for their assistance on drawing the schemes.

Received: October 19, 2013
Revised: November 12, 2013
Published online: December 21, 2013

[1] a) P. Coullet, L. Gil, F. Rocca, *Opt. Commun.* **1989**, *73*, 403; b) J. Verbeeck, H. Tian, G. Van Tendeloo, *Adv. Mater.* **2013**, *25*, 1114.
[2] L. Allen, M. W. Beijersbergen, R. J. C. Spreeuw, J. P. Woerdman, *Phys. Rev. A* **1992**, *45*, 8185.
[3] G. Molina-Terriza, J. P. Torres, L. Torner, *Nat. Phys.* **2007**, *3*, 305.
[4] A. M. Yao, M. J. Padgett, *Adv. Opt. Photon.* **2011**, *3*, 161.
[5] J. P. Torres, L. Torner, *Twisted photons, applications of light with orbital angular momentum*, Wiley-VCH, Weinheim, Germany **2011**.
[6] A. Mair, A. Vaziri, G. Weihs, A. Zeilinger, *Nature* **2001**, *412*, 313.
[7] a) S. Franke-Arnold, L. Allen, M. Padgett, *Laser Photon. Rev.* **2008**, *2*, 299; b) B. Jack, A. M. Yao, J. Leach, J. Romero, S. Franke-Arnold, D. G. Ireland, S. M. Barnett, M. J. Padgett, *Phys. Rev. A* **2010**, *81*, 043 844.
[8] J. Wang, J. Y. Yang, I. M. Fazal, N. Ahmed, Y. Yan, H. Huang, Y. X. Ren, Y. Yue, S. Dolinar, M. Tur, A. E. Willner, *Nat. Photon.* **2012**, *6*, 488.
[9] a) Y. Zhao, J. S. Edgar, G. D. M. Jeffries, D. McGloin, D. T. Chiu, *Phys. Rev. Lett.* **2007**, *99*, 073 901; b) X. L. Wang, J. Chen,

Y. N. Li, J. P. Ding, C. S. Guo, H. T. Wang, *Phys. Rev. Lett.* **2010**, *105*; c) Y. Hong, M. Pourmand, S. V. Boriskina, B. M. Reinhard, *Adv. Mater.* **2013**, *25*, 115.
[10] G. Foo, D. M. Palacios, G. A. Swartzlander, *Opt. Lett.* **2005**, *30*, 3308.
[11] J. M. Vaughan, D. V. Willetts, *Opt. Commun.* **1979**, *30*, 263.
[12] a) M. W. Beijersbergen, R. P. C. Coerwinkel, M. Kristensen, J. P. Woerdman, *Opt. Commun.* **1994**, *112*, 321; b) S. S. R. Oemrawsingh, J. A. W. van Houwelingen, E. R. Eliel, J. P. Woerdman, E. J. K. Verstegen, J. G. Kloosterboer, G. W. Hooft, *Appl. Opt.* **2004**, *43*, 688; c) K. Sueda, G. Miyaji, N. Miyanaga, M. Nakatsuka, *Opt. Express* **2004**, *12*, 3548; d) X. C. Yuan, J. Lin, J. Bu, R. E. Burge, *Opt. Express* **2008**, *16*, 13 599.
[13] M. Uchida, A. Tonomura, *Nature* **2010**, *464*, 737.
[14] a) L. Marrucci, C. Manzo, D. Paparo, *Phys. Rev. Lett.* **2006**, *96*, 163 905; b) D. Ganic, X. S. Gan, M. Gu, M. Hain, S. Somalingam, S. Stankovic, T. Tschudi, *Opt. Lett.* **2002**, *27*, 1351.
[15] S. Slussarenko, A. Murauski, T. Du, V. Chigrinov, L. Marrucci, E. Santamato, *Opt. Express* **2011**, *19*, 4085.
[16] A. V. Carpentier, H. Michinel, J. R. Salgueiro, D. Olivieri, *Am. J. Phys.* **2008**, *76*, 916.
[17] a) V. Y. Bazhenov, M. V. Vasnetsov, M. S. Soskin, *JETP. Lett.* **1990**, *52*, 429; b) V. Y. Bazhenov, M. S. Soskin, M. V. Vasnetsov, *J. Mod. Opt.* **1992**, *39*, 985; c) N. R. Heckenberg, R. McDuff, C. P. Smith, H. Rubinszteindunlop, M. J. Wegener, *Opt. Quantum. Electron* **1992**, *24*, S951.
[18] a) Q. Li, *Liquid Crystals Beyond Displays: Chemistry, Physics, and Applications* John Wiley & Sons, **2012**; b) T. H. Lin, Y. N. Li, C. T. Wang, H. C. Jau, C. W. Chen, C. C. Li, H. K. Bisoyi, T. J. Bunning, Q. Li, *Adv. Mater.* **2013**, *25*, 5050; c) Q. Li, Y. Li, J. Ma, D. K. Yang, T. J. White, T. J. Bunning, *Adv. Mater.* **2011**, *23*, 5069.
[19] E. Brasselet, N. Murazawa, H. Misawa, S. Juodkazis, *Phys. Rev. Lett.* **2009**, *103*, 103 903.
[20] Y. J. Liu, X. W. Sun, D. Luo, Z. Raszewski, *Appl. Phys. Lett.* **2008**, *92*, 101114.
[21] a) Y. J. Liu, X. W. Sun, Q. Wang, D. Luo, *Opt. Express* **2007**, *15*, 16 645; b) M. Infusino, A. De Luca, V. Barna, R. Caputo, C. Umeton, *Opt. Express* **2012**, *20*, 23 138.
[22] a) N. R. Heckenberg, R. McDuff, C. P. Smith, A. G. White, *Opt. Lett.* **1992**, *17*, 221; b) A. Jesacher, C. Maurer, A. Schwaighofer, S. Bernet, M. Ritsch-Marte, *Opt. Express* **2008**, *16*, 2597.
[23] a) M. Schadt, H. Seiberle, A. Schuster, *Nature* **1996**, *381*, 212; b) W. Y. Wu, A. Y. G. Fuh, *Jpn. J. Appl. Phys.* **2007**, *46*, 6761; c) S. R. Nersisyan, N. V. Tabiryan, D. M. Steeves, B. R. Kimball, V. Chigrinov, H. S. Kwok, *Appl. Opt.* **2010**, *49*, 1720; d) A. Priimagi, M. Saccone, G. Cavallo, A. Shishido, T. Pilati, P. Metrangolo, G. Resnati, *Adv. Mater.* **2012**, *24*, OP345.
[24] a) N. Kawatsuki, T. Tachibana, K. Kamada, *Adv. Mater.* **2005**, *17*, 1886; b) X. Zhao, A. Bermak, F. Boussaid, T. Du, V. G. Chigrinov, *Opt. Lett.* **2009**, *34*, 3619.
[25] H. Wu, W. Hu, H. C. Hu, X. W. Lin, G. Zhu, J. W. Choi, V. Chigrinov, Y. Q. Lu, *Opt. Express* **2012**, *20*, 16 684.
[26] a) W. Hu, A. Srivastava, X. W. Lin, X. Liang, Z. J. Wu, J. T. Sun, G. Zhu, V. Chigrinov, Y. Q. Lu, *Appl. Phys. Lett.* **2012**, *100*, 111 116; b) W. Hu, A. Srivastava, F. Xu, J. T. Sun, X. W. Lin, H. Q. Cui, V. Chigrinov, Y. Q. Lu, *Opt. Express* **2012**, *20*, 5384.
[27] X. W. Lin, W. Hu, X. K. Hu, X. Liang, Y. Chen, H. Q. Cui, G. Zhu, J. N. Li, V. Chigrinov, Y. Q. Lu, *Opt. Lett.* **2012**, *37*, 3627.
[28] J. Sun, S. Xu, H. Ren, S. T. Wu, *Appl. Phys. Lett.* **2013**, *102*, 161 106.
[29] A. K. Srivastava, W. Hu, V. G. Chigrinov, A. D. Kiselev, Y. Q. Lu, *Appl. Phys. Lett.* **2012**, *101*, 031 112.